



Research Article

Cost-effective ZnO–Eu³⁺ films with efficient energy transfer between host and dopant

Archana Singh¹ · Priyanka Arya¹ · Diksha Choudhary¹ · Surender Kumar¹ · A. K. Srivastava¹ · I. B. Singh¹

Received: 2 August 2019 / Accepted: 2 April 2020 / Published online: 10 April 2020
© Springer Nature Switzerland AG 2020

Abstract

The present work focuses on the deposition of Europium (Eu³⁺) incorporated zinc oxide (ZnO) film by a cost effective chemical solution deposition method. ZnO film with varying concentration of Eu³⁺ ions (2, 3 and 4 atomic percent) were deposited and characterized using different techniques like X-ray diffractogram (XRD), scanning electron microscopy. XRD studies revealed that highly *c*-axis oriented ZnO films without showing any segregation of europium oxide were obtained at 650 °C. The optical properties were determined using UV–visible spectrophotometry and photoluminescence measurements. UV-visible spectroscopy revealed that Eu³⁺ doping shifted optical band gap with increase in transparency of the films. The Eu³⁺ doped film showed intense emission at 614 nm which was attributed to the defect emission from ZnO that gets trapped by Eu³⁺ ions ultimately leading to ⁷F₂ to ⁵D₀ transition in Eu³⁺.

Keywords Thin films · Eu-doped zinc oxide · Sol–gel · XRD · Optical absorption · PL

1 Introduction

ZnO, because of its direct wide band gap of 3.37 eV, a large exciton binding energy (60 meV) [1], superior chemical stability [2] and unique optical properties, has triggered a vast research area for both fundamental and technological reasons [3–7]. Doping in ZnO with selective element as well as intrinsic lattice defects greatly influence its electronic, optical and magnetic properties either in film or powder form [8–13]. Doped ZnO films have attracted much attention because of their wide applications such as photoactive material for short wavelength light emitting devices, piezoelectric transducers, optoelectronic devices and transparent conducting electrodes [14–17]. Under proper excitation conditions, ZnO exhibits two kinds of emissions, one is an ultraviolet (UV) near band edge emission at 380 nm and other is a visible deep level emission with a peak in range from 450–730 nm [18, 19]. By doping ZnO with luminescence centre such as trivalent rare earth elements it is possible to enlarge the palette of

colors emitted by it and also to tune its emission properties, which would be greatly beneficial for light emitting device applications such as plasma display panels, multi color emission in light emitting devices [20–23]. To achieve efficient luminescence of ZnO–RE³⁺ enhance energy transfer from semiconductor host to RE³⁺ is required, but due to large ionic radii difference between two and also charge mismatching results are often disappointing.

ZnO based films have been prepared by number of different techniques like spray pyrolysis [24], electrodeposition [8], pulsed laser deposition [25], sputtering [26], sol–gel [11, 13, 27, 28] and metal organic chemical vapor deposition method [29]. Among them, sol–gel method has distinct potential advantage over the other due to its ability to control micro structure by sol gel chemistry, highly economical and its room temperature approach. By controlling parameters like solvent nature, precursor nature and concentration, preheating temperature and time, post annealing temperature it is possible to obtain good quality thin films with good control over chemical

✉ Archana Singh, archanas002@gmail.com | ¹Advanced Materials and Processes Research Institute, Bhopal, India.



composition, morphology and microstructure [13]. Peterson and group reported the Eu-doped ZnO film deposition on silicon substrate using sol–gel process, though the films deposited do not possess a good structural quality, with the accumulation of europium at the film surface. Raji et al. synthesized the ZnO–Eu³⁺ nanostructure powder using coprecipitation method [30]. They reported that Eu³⁺ incorporation changed the morphology of the nanostructure from rod to flower. The energy transfer between the ZnO and Eu³⁺ was attributed to the defect mediated process. Zhang and group reported the Eu³⁺ doped ZnO nanospheres by wet chemical method [31]. They observed white emission by doping Eu³⁺ in ZnO nanospheres and showed detailed energy transfer process from ZnO to Eu³⁺. Yu et al. synthesized ZnO–Eu³⁺ nanoflowers at a low temperature by hydrothermal method [32]. They reported that on excitation of Eu³⁺, emission showed presence of Eu³⁺ at different sites one of which is similar to Eu³⁺ in C-type Eu₂O₃. ZnO–Eu³⁺ doped nanostructure were prepared by combustion method. However they reported very weak visible emission intensity of Eu³⁺ [33].

This present work demonstrates the polymer assisted deposition of Eu-doped ZnO films using chemical solution deposition method on quartz substrate. The structural and the optical properties of the films were studied using XRD, scanning electron microscopy (SEM) and PL spectroscopy. Our results show that the deposited films possess homogeneous and uniform structure with efficient energy transfer between ZnO and Eu³⁺

2 Experimental

Eu³⁺ doped and undoped ZnO films were prepared on chemically cleaned quartz substrate. Biodegradable polymer polyvinyl alcohol (PVA) and zinc acetate dihydrate (Zn–(CH₃COO)₂·2H₂O) were used for sol solution. To prepare a sol 1.65 g of Zinc acetate dehydrate (SD Fine Chemicals) and 1.65 g of PVA (mol. wt. 125,000, SD Fine) were added to 60 ml of deionised water, which was then heated to 45 °C for 1 h with constant stirring. For rare earth doped samples three different Eu³⁺ concentrations (2, 3 and 4 at%) were selected. Europium III nitrate (Aldrich chemicals) was used as Eu³⁺ source. The mixed sol was stirred continuously until all reagents were dissolved completely. The sol was then spin coated on cleaned quartz substrate at 3500 rpm for 30 s and films were then dried at 120 °C on hot plate after each coating. The above process was repeated for six times to get film of desired thickness. Finally ZnO films were annealed at 450, 550 and 650 °C for 1 h in air.

Films were subjected to X-Ray diffraction studies with Cu–K_α radiation (1.54 Å). The diffractometer (FRL XTRA,

Thermoelectron) was operated at 40 kV and 35 mA with a glancing angle of 1°. Optical absorption study was carried out in wavelength range of 300–700 nm using Perkin elmer spectrometer. PL spectra were measured at room temperature with an excitation source of 325 and 465 nm using Fluorolog@-3, JOBIN YVON HORIBA group instrument. SEM images of samples were obtained using FEI Quanta 200, The Netherlands SEM.

3 Result and discussion

3.1 Structural properties

Structural evolution of the ZnO films as a function of annealing temperature was investigated by XRD analysis is shown in Fig. 1. All the patterns indicate the formation of wurtzite type ZnO phase with strong c-axis orientation. With the increase in annealing temperature crystallinity and orientation of films along c-axis increases. Relatively higher XRD peak intensity has been observed for samples annealed at 650 °C. The full width at half maxima (FWHM) of films also decreased with increasing temperature, which indicates that crystallinity of the films have been improved on annealing. The c-axis orientation in film can be explained by “survival of the fittest model” [30]; nucleation with various orientation can be formed at the initial stage of deposition and each nucleus competes to grow, but only having the fastest growth rate can survive. The small surface free energy for (002) planes [34] of ZnO accounts for its fastest growth at higher temperature. Therefore as annealing temperature increases films preferably grow along (002) direction.

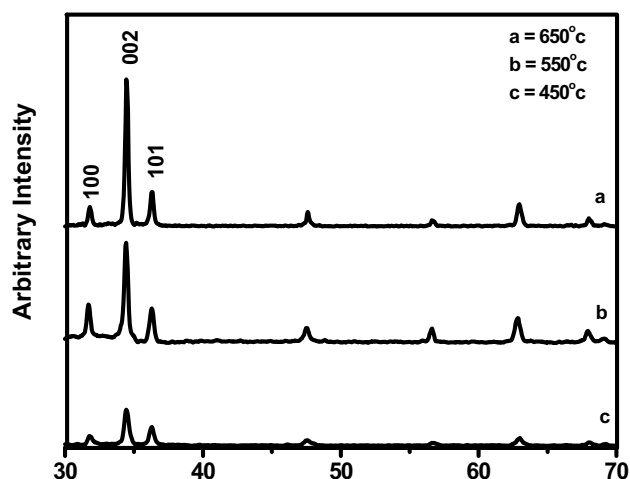


Fig. 1 X-ray diffraction pattern of pure ZnO films annealed at 650 °C (a), 550 °C (b) and 450 °C (c)

Figure 2A shows the XRD pattern of films as a function of Eu^{3+} concentration (2, 3 and 4 at%) annealed at 650 °C. All films show hexagonal wurtzite structure and preferred growth along 002 plane. However preferred orientation along (002) plane decreases with increase of Eu^{3+} concentration. Lines due to different crystalline phases such as europium oxides or hydroxides were not detected in diffraction pattern of samples annealed at this temperature, thus suggesting homogenous dispersion of dopant in ZnO matrix. Higher thermal treatment of 850 °C did not induce any change in wurtzite phase of these films however a weak peak at 2 theta = 28.4° (shown in Fig. 2B) appeared. This peak was indexed as the (222) reflection of bcc structure of Eu_2O_3 , similar result has also been observed in Eu^{3+} doped ZnO nanopowders [9]. This shows that high annealing condition promotes the aggregation of Eu^{3+} centers and crystallization of Eu_2O_3 clusters. The large lattice energy difference between ZnO (412 kJ/mol and Eu_2O_3 (12,945 kJ/mol) may cause phase separation in sample at higher temperature. Tendency of rare earth element to segregate at ZnO grain boundary in lanthanum (La) doped ZnO system has already been reported [35, 36]. Further characterizations have been carried out on films annealed at 650 °C. Inset of Fig. 2A shows the XRD pattern of doped ZnO films in range of 33°–35.5°. The diffraction pattern shows shift in 002 peaks to smaller angle with increase in Eu^{3+} concentration. It indicates incorporation of some of the Eu^{3+} ions in ZnO lattice although there is large ionic radii difference between Zn^{2+} (60 pm) and Eu^{3+} (94.7 pm) [9].

The lattice constants and volume of unit cell shows linear increase with increase in dopant concentration which is attributed to Eu^{3+} dopant (Fig. 3A). Eu^{3+} incorporation

will result in expansion of ZnO lattice. Figure 3B displays variation of FWHM of 002 diffraction peak along with mean grain size normal to 002 plane estimated by scherrer's formula. FWHM of 002 peaks become broad and increase monotonically with dopant concentration which indicates that film crystallization has deteriorated. The grain size also decreases (85 nm) from undoped to (49.11 nm) for 4% doped samples (Table 1). It has been reported that dopant with smaller ionic radii have good diffusivity and they prefer oriented growth and good crystallization but difference in ionic radii makes diffusivity of ions difficult and leads to the formation of stress in lattice [37]. In our system also due to large difference in ionic size and charge between Eu^{3+} ($r=94.7$ pm, CN=6) and Zn^{2+} ($r=60$ pm, CN=4) the doping of Eu^{3+} deteriorates crystallization of films Also segregation of Eu_2O_3 in grain boundary may inhibit the combination of ZnO grains and thereby decrease grain size.

Effect of doping on preferential orientation of the films was studied by calculating texture coefficient $\text{TC}_{(hkl)}$ for all the planes using following equation [38, 39].

$$\text{TC}_{hkl} = \frac{I_{hkl}}{I_{0hkl}} \left[\frac{1}{N} \sum \frac{I_{hkl}}{I_{0hkl}} \right] \quad (1)$$

where $\text{TC}_{(hkl)}$ is the texture coefficient of (hkl) plane, I the measured diffraction intensity, I_0 the standard intensities measured from randomly oriented powder samples and N is the number of reflections observed in the X-ray diffraction pattern. The deviation of texture coefficient from unity indicates preferred orientation of the growth. Figure 3C shows the $\text{TC}_{(hkl)}$ values for typical planes of doped and undoped films which clearly imply formation of c-axis

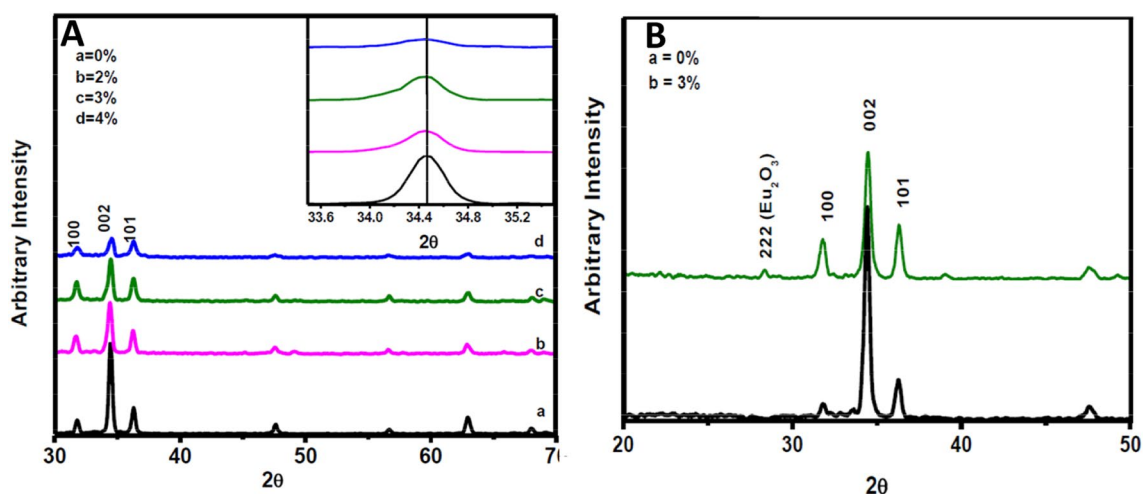


Fig. 2 **a** X-ray diffraction pattern of ZnO films deposited using various doping concentration (at%) of Eu annealed at 650 °C inset of shows, XRD pattern of undoped ZnO and Eu-doped ZnO films

between 2θ value of 33.5°–35.5°. **b** XRD pattern obtained for ZnO (a) and 3 at % Eu-doped ZnO film annealed at 850 °C

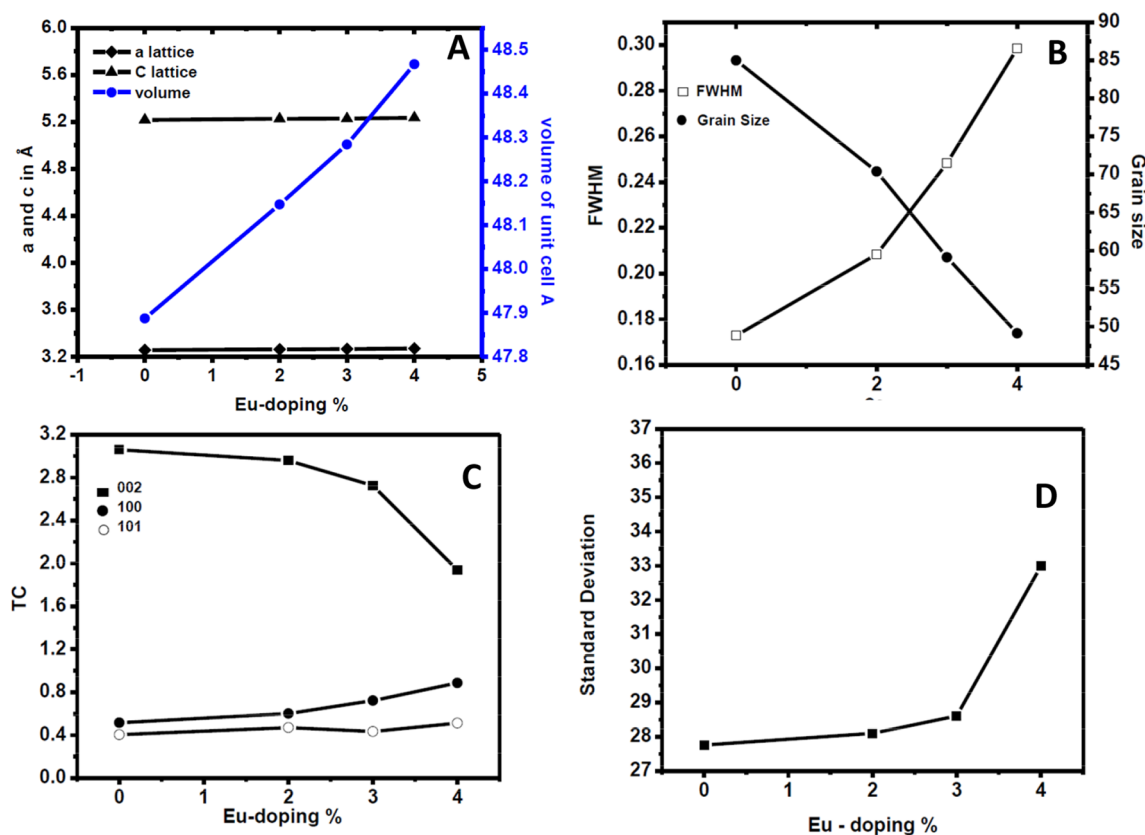


Fig. 3 **a** Lattice parameter (a and c) and cell volume of pure and cell volume of pure and Eu-doped ZnO films. **b** FWHM value of (002) peak and grain size of ZnO films as a function of Eu-dop out concentration. **c** TC (002), TC (001) and TC (101) plotted against dop-

ing concentration of Eu^{3+} for films anneal at $650\text{ }^\circ\text{C}$. **d** Variation of standard deviation in intensity of XRD peaks wrt doping concentration of Eu^{3+} for the films deposited at $650\text{ }^\circ\text{C}$

Table 1 Lattice parameters and unit cell volumes for pure and Eu incorporated ZnO systems

Eu (at %)	a (Å)	c (Å)	V (Å) ³	Grain size(nm)	TC ₀₀₂	TC ₁₀₁	TC ₁₀₀	σ
0	3.256	5.216	47.887	85.00	3.062	0.404	0.516	27.76
2	3.262	5.225	48.147	70.40	2.958	0.470	0.602	28.61
3	3.266	5.227	48.284	59.10	2.725	0.433	0.722	28.10
4	3.270	5.234	48.467	49.11	1.939	0.712	0.839	32.99

oriented films. However with the increase in Eu^{3+} concentration TC₍₀₀₂₎ value slightly decreases but after 3% doping TC₍₀₀₂₎ value sharply decreases that shows deviation from preferred (002) direction. Growth mechanism of the film can be studied by calculating standard deviation (σ) using the equation [37].

$$\sigma = \sqrt{\frac{\sum I_{hkl}^2 - (\sum I_{(hkl)})^2 / N}{N}} \tag{2}$$

where I stands for relative intensity of a (h k l) plane.

From Fig. 3D it can be seen that there is small change in sigma values up to 3% which shows onset of homogeneous nucleation up to this doping level while a relatively

higher value for 4% which is attributed to deviation from preferred orientation. This may be because beyond certain doping level further heavy doping makes it difficult to form a critical nucleus to develop along a particular direction and random orientation seems to be preferred (Table 1).

Figure 4a, b, c and d shows surface morphology of undoped and Eu^{3+} doped (2, 3, 4%) ZnO thin films. Samples show compact, smooth and polycrystalline morphology. It can be seen that there are no cracks or peels in the films. Grain boundaries can be clearly seen. The grain size of undoped film is larger than those of Eu^{3+} doped films, which indicates that Eu^{3+} suppresses the growth of grains. Pure ZnO film shows a loose structure containing large

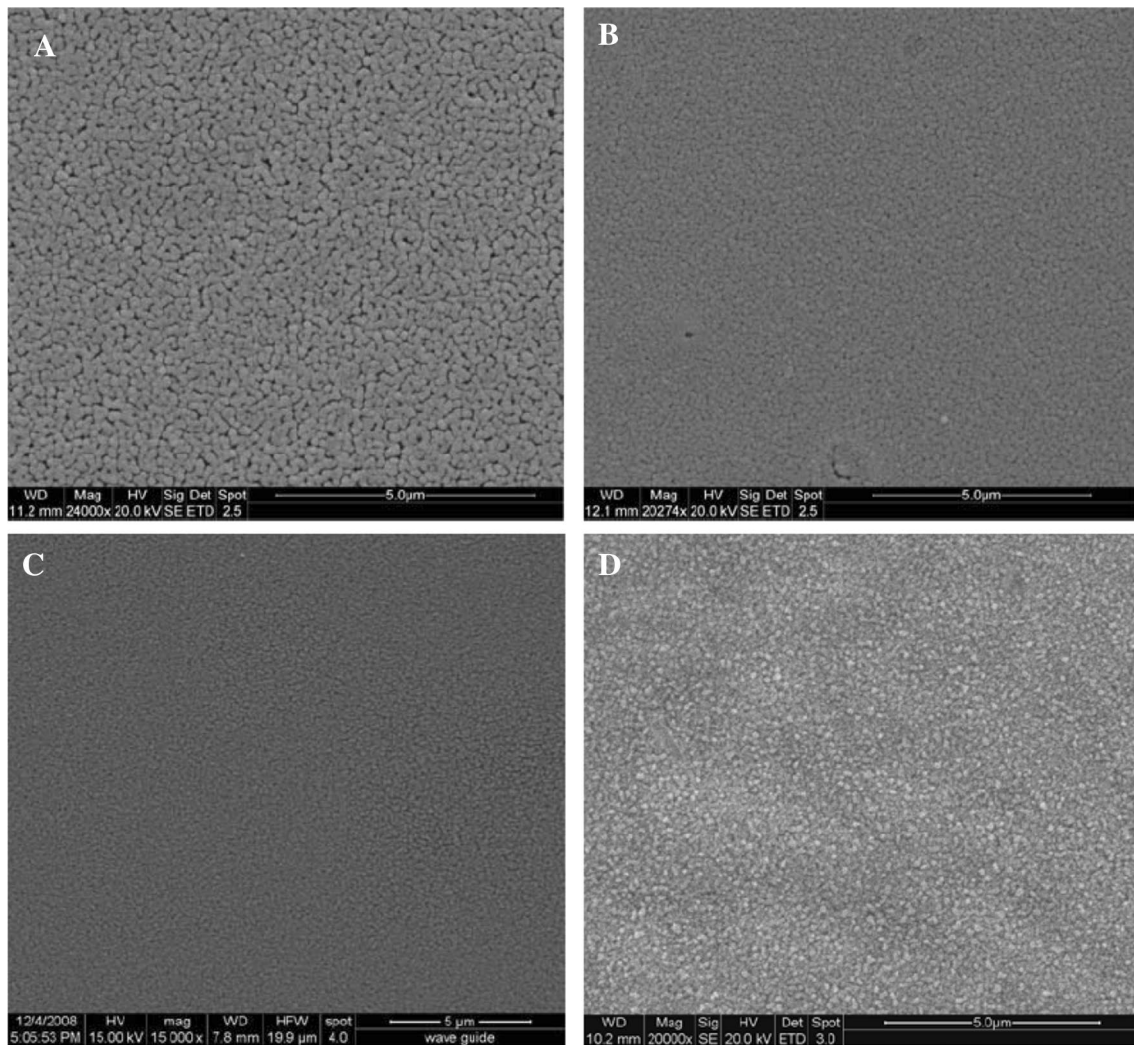


Fig. 4 SEM images of ZnO and Eu-doped ZnO films with different Eu concentration; **a** (0%), **b** (2 at%), **c** (3 at%), **d** (4 at%)

grains whereas doped ZnO possess small grains. Small pores can also be seen in undoped film that may be due to evaporation of water while doped film shows denser and tightly packed structure. These results are consistent with XRD pattern were obtained. These SEM images imply that the surface morphology of the films is strongly dependent on the concentration of dopant.

3.2 Optical properties

Optical transmission spectra for undoped and doped films are shown in Fig. 5. Films are highly transparent in visible region. Eu^{3+} doping increased the transparency of films due to broadening of optical band gap. For optical band gap, optical absorption coefficient (α) of direct band gap semiconductor ZnO can be obtained by following equation [10],

$$\alpha = A(h\nu - E_g)^{1/2} \quad (3)$$

where A is the proportionality constant, h is photon energy and E_g is optical band gap. The transmittance T , near the absorption edge, is given by

$$T \cong \exp(-\alpha d) \quad (4)$$

where d is thickness of films. Also α is proportional to $(\ln T)$ [2, 40, 41]

$$(\ln T)^2 \mu a^2 d^2 = A^2 d^2 ((h\nu - E_g)) \quad (5)$$

Thus plotting $(\ln T)^2$ as a function of the photon energy and drawing a tangential line near the absorption edge, one can determine the optical band gap. Figure 5b shows $(\ln T)^2$ vs h plots for undoped and doped films. The undoped ZnO films exhibit E_g values of 3.226 eV while E_g values for the 2, 3 and 4% doped ZnO films were found to

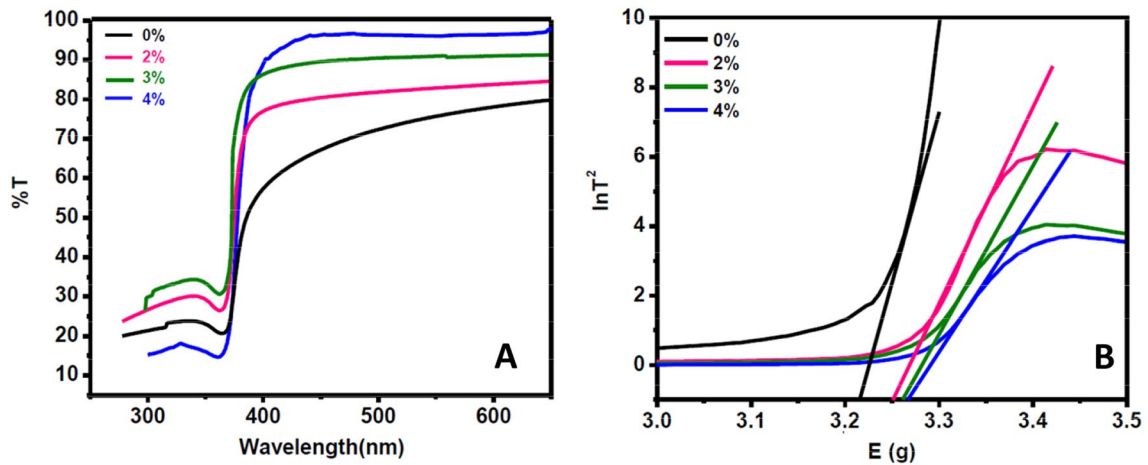


Fig. 5 **a** Optical transmittance of pure ZnO, **b** square of $\ln T$ (T =transmittance) vs photon energy for undoped and doped ZnO films

be 3.248, 3.261 and 3.266 eV. It is clear that optical band gap increases with increase of Eu^{3+} concentration. The blue shift of the band gap is caused by Eu^{3+} ion incorporated in the ZnO lattice. This is consistent with XRD results.

The photoluminescence (PL) of ZnO film was studied under an excitation of 325 nm (Fig. 6a). First peak is observed at 390 nm which is attributed to recombination of bound excitons in ZnO. The second broad band

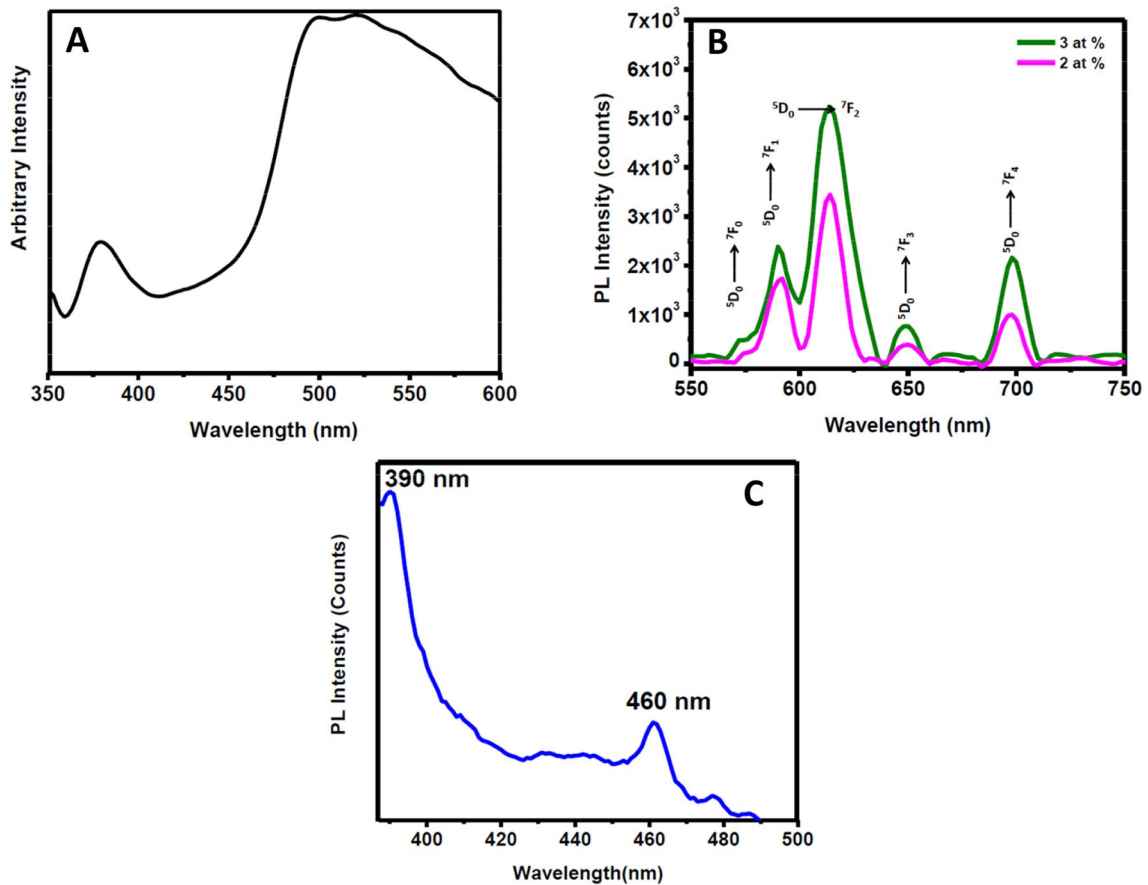


Fig. 6 **a** PL of ZnO film recorded at excitation of 325 nm. **b** PL spectra of 2% and 3% Eu-doped ZnO films at the excitation wavelength of 464 nm, **c** figure shows the PL of the 3% Eu-doped ZnO film annealed at 650 °C at excitation wavelength of 614 nm

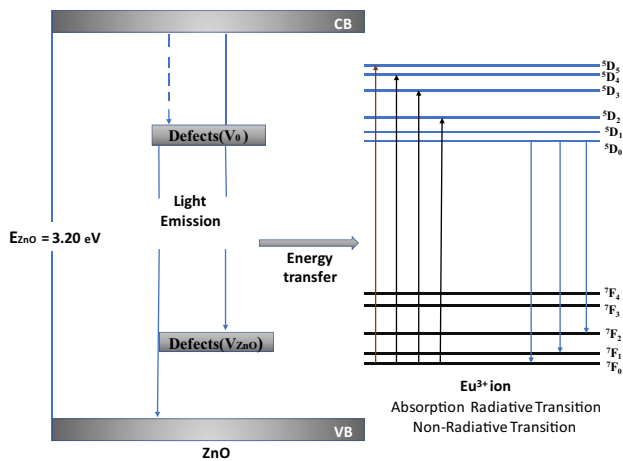


Fig. 7 Possible emission and excitation path ways in ZnO and Eu doped ZnO

is observed at 510 nm which can be assigned to oxygen vacancies. Eu-doped films were studied by exciting in 5D_2 multiplet at 464 nm. Figure 6b shows the PL spectra of 2 and 3% doped films. Emission peaks were observed at 576, 591, 614, 649 and 699 nm, which can be assigned to the transitions from the 5D_0 (Eu^{3+}) excited state to the 7F_J (with $J=0, 1, 2, 3, 4$) multiplets, respectively. With the increase in concentration of Eu^{3+} intensities of peak increased [42, 43].

On absorption of excitation energy ZnO electrons get promoted to the conduction band from the valence band. The excited electrons get trapped by various defect sites via process of radiative decay. Now UV emission results due to the recombination of holes in the valence band with the electrons in defect states. In presence of Eu^{3+} in the ZnO lattice, a segment of recombination energy is captured by the Eu^{3+} ion that excites electron from the ground state of Eu^{3+} ion to excited state. These electron results in Eu^{3+} emission by radiative relaxation. This has been reported in the literature that the intensity of the Eu^{3+} emission depends on the charge carrier and energy transfer process. In present work, we propose that defect emission from the ZnO is trapped by Eu^{3+} ions which excite 7F_J to 5D_0 transition in Eu^{3+} . These electrons get transfer from 5D_J state to 7F_J state of Eu^{3+} leading to light emission (Fig. 7).

Appearance of forbidden transition i.e. 5D_0 to 7F_0 implies that there is reduction of local symmetry around Eu^{3+} ions. This may be because Eu^{3+} ions occupy the grain boundaries of ZnO. Now the grain boundaries have broken bonds in Zn–O or Eu–O and it has less M–O coordination number. Due to this local symmetry on Eu^{3+} ion is reduced. Figure 6b also shows that intensity of forbidden transition peak increased on increasing dopant concentration which shows further decrease of symmetric environment. Also 5D_0 to 7F_2 transition peak get broadened for the 4% doped

films that is attributed to decreased crystal quality of films on increasing dopant concentration which is in accordance with XRD results. The excitation spectra of 3% Eu^{3+} doped film for λ_{exc} 614 nm shown in Fig. 6C. As can be seen that two prominent peak at 465 nm for excitation 7F_0 – 5D_2 and a strong peak at 395 nm of direct 7F_0 – 5D_6 excitation was obtained. This peak at 395 nm overlaps with the emission due to ZnO only which is observed around 390 nm. Similar observation was also reported for the ZnO– Eu^{3+} nanoparticles where efficient energy transfer was reported between ZnO and Eu^{3+} [43].

Y_2O_3 – Eu^{3+} and YVO_4 – Eu^{3+} materials are well known red emitting phosphors [44–47]. YVO_4 – Eu^{3+} shows a strong 5D_0 to 7F_2 transition because of efficient energy transfer from VO_4^{3-} to Eu^{3+} [45]. Similarly Y_2O_3 – Eu^{3+} shows a strong red emission from Eu^{3+} via Eu^{3+} – O^{2-} charge transfer and Y^{3+} – O^{2-} excitonic electron transfer mechanism. These oxides and systems shows f–f transitions as well [46]. In ZnO– Eu^{3+} , after excitation the carriers get relaxed and are caught by defects or results in radiative emission. However the red emission from the composite involving cheap and abundant metal oxides like ZnO is desirable.

4 Conclusion

Eu^{3+} doped and undoped ZnO thin films are prepared by metal-organic decomposition method. Doping of Eu^{3+} does not change the wurtzite structure of ZnO films, however it deteriorates crystallinity of ZnO films and also it reduces the orientation of film along c-axis orientation. Grain size decreases as the Eu^{3+} content increases in film. Doping of Eu^{3+} increased the transparency of films in visible region and also increase energy band gap from 3.20 eV for undoped film to 3.23 eV for 4% doped film, it is because of incorporation of some of the Eu^{3+} ion in ZnO film. Emission spectrum at the excitation wavelength of 464 nm for doped films also confirms the incorporation of Eu^{3+} ions in ZnO films. Excitation spectrum shows the efficient energy transfer between ZnO and Eu^{3+} .

Acknowledgements The authors acknowledge the director CSIR-AMPRI, for allowing to carry out the project. One of the authors A.S acknowledge the INSPIRE faculty award (IFA13CH112) and Alexander Humboldt Foundation for the AVH postdoctoral fellowship for the financial assistance.

Compliance with ethical standards

Conflict of interest The author(s) declare that they have no competing interests.

References

- Ahmed S, Szymanski P, El-Nadi L (2014) Energy-transfer efficiency in Eu-doped ZnO thin films: the effects of oxidative annealing on the dynamics and the intermediate defect states. *ACS Appl Mater Interfaces* 6(3):1765–1772. <https://doi.org/10.1021/am404662k>
- Konenkamp R, Word R, Godinez M (2005) Ultraviolet electroluminescence from ZnO/polymer heterojunction light-emitting diodes. *Nanoletter* 10:2005–2008. <https://doi.org/10.1021/nl051501r>
- Ozgur U, Alivov Y, Teke A, Reschikoy M, Dogan S, Avrutin V, Cho S, Morkoc H (2005) A comprehensive review of ZnO materials and devices. *J Appl Phys* 98:41301. <https://doi.org/10.1063/1.1992666>
- Che P, Meng J, Guo L (2007) Oriented growth and luminescence of ZnO:Eu films prepared by sol–gel process. *J Lumin* 122:168–171. <https://doi.org/10.1016/j.jlumin.2006.01.076>
- Kossanyi J, Kouyate D, Pouliquen J, Ronfard-Haret J, Valat P, Oelkrug D, Mammel U, Kelly G, Wilkinson F (1990) Photoluminescence of semiconducting zinc oxide containing rare earth ions as impurities. *J Lumin* 46:17–24. [https://doi.org/10.1016/0022-2313\(90\)90077-0](https://doi.org/10.1016/0022-2313(90)90077-0)
- Kouyate D, Ronfard-Haret J, Kossanyi J (1991) Photo- and electro-luminescence of rare earth-doped semiconducting zinc oxide electrodes: emission from both the dopant and the support. *J Lumin* 50:205. [https://doi.org/10.1016/0022-2313\(91\)90044-V](https://doi.org/10.1016/0022-2313(91)90044-V)
- Yoon K, Cho J (2000) Photoluminescence characteristics of zinc oxide thin films prepared by spray pyrolysis technique. *Mater Res Bull* 35:39–46. [https://doi.org/10.1016/S0025-5408\(00\)00183-5](https://doi.org/10.1016/S0025-5408(00)00183-5)
- Pauporte T, Pelle F, Viana B, Aschehoug P (2007) Luminescence of nanostructured $\text{Eu}^{3+}/\text{ZnO}$ mixed films prepared by electrodeposition. *J Phys Chem C* 111:15427–15432. <https://doi.org/10.1021/jp0747860>
- Armelaio L, Bottaro G, Pascolini M, Sessolo M, Tondello E, Bettinelli M, Speghini A (2008) Structure–luminescence correlations in europium-doped sol–gel ZnO nanopowders. *J Phys Chem C* 112:4049–4054. <https://doi.org/10.1021/jp710207r>
- Fujihara S, Ogawa Y, Kasai A (2004) Tunable visible photoluminescence from ZnO thin films through Mg-doping and annealing. *Chem Mater* 16:2965–2971. <https://doi.org/10.1021/cm049599i>
- Zhang Y, Zhang Z, Lin B, Fu Z, Xu J (2005) Effects of Ag doping on the photoluminescence of ZnO films grown on Si substrates. *J Phys Chem B* 109(41):19200–19203. <https://doi.org/10.1021/jp0538058>
- Han S, Jang T, Kim Y, Park B, Park J, Jeong Y (2004) Exchange bias and the origin of magnetism in Mn-doped ZnO tetrapods. *Appl Phys Lett* 85:2589–2595. <https://doi.org/10.1063/1.1795366>
- Petersen J, Brimont C, Gallart M, Schmerber G, Gilliot P, U-Bouillet C, Rehspringer J, Coils S, Becker C, Slaoui A, Dinia A (2010) Correlation of structural properties with energy transfer of Eu-doped ZnO films prepared by sol-gel process and magnetron sputtering. *J Appl Phys* 107:123522–123530. <https://doi.org/10.1063/1.3436628>
- Thomas D (1960) The exciton spectrum of zinc oxide. *J Phys Chem Solids* 16:86–96. [https://doi.org/10.1016/0022-3697\(60\)90104-9](https://doi.org/10.1016/0022-3697(60)90104-9)
- Joseph M, Tabata H, Kawai T (1999) Ferroelectric behavior of Li-doped ZnO thin films on Si(100) by pulsed laser deposition. *Appl Phys Lett* 74:2534–2540. <https://doi.org/10.1063/1.123889>
- Perez-casero R, Gutierrez-Llorente A, Mollwilfrid O, Defourneau S, Defourneau D (2005) Er-doped ZnO thin films grown by pulsed-laser deposition. *J Appl Phys* 97:054905–054911. <https://doi.org/10.1063/1.1858058>
- Armelaio L, Heigl F, Jurgensen A, Blyth R, Regier T, Zhou X, Sham T (2007) X-ray excited optical luminescence studies of ZnO and Eu-doped ZnO nanostructures. *J Phys Chem C* 111:10194–10201. <https://doi.org/10.1021/jp071379f>
- Kar S, Dev A, Chaudhuri S (2006) Simple solvothermal route to synthesise ZnO nanosheets, nanonails and well aligned nanorod arrays. *J Phys Chem B* 110:17848–17853. <https://doi.org/10.1021/jp0629902>
- Nyffenegger R, Craft B, Shaaban M, Gorer S, Erley G, Penner R (1998) A hybrid electrochemical/chemical synthesis of zinc oxide nanoparticles and optically intrinsic thin films. *Chem Mater* 10:1120–1129. <https://doi.org/10.1021/cm970718m>
- Gao S, Zhang H, Deng R, Wang X, Sun D, Zheng G (2006) Engineering white light-emitting Eu-doped ZnO urchins by biopolymer-assisted hydrothermal method. *Appl Phys Lett* 89:123125–123132. <https://doi.org/10.1063/1.2357031>
- Chen L, Zhang J, Zhang X, Liu F, Wang X, (2008) Optical properties of trivalent europium doped ZnO:Zn phosphor under indirect excitation of near-UV light. *Opt Express* 16(16):11795–11801. <https://doi.org/10.1364/OE.16.011795>
- Lima SAM, Sigoli FA, Davolos MR, Jafelicci M Jr (2002) Europium (III)-containing zinc oxide from Pechini method. *J Alloys Compd* 344(1):280–284. [https://doi.org/10.1016/S0925-8388\(02\)00369-9](https://doi.org/10.1016/S0925-8388(02)00369-9)
- Abdullah M, Morimoto T, Okuyama K (2003) Generating blue and red luminescence from ZnO/poly(ethylene glycol) nanocomposites prepared using an in-situ method. *Adv Funct Mater* 13(10):800–804. <https://doi.org/10.1002/adfm.200304330>
- Pauporte T, Goux A, Kahn-Harari A, de Tacconi N, Chenthamarashan R, Rajeshwar K, Lincot D (2003) Cathodic electrodeposition of mixed oxide thin films. *J Phys Chem Solids* 64(9):1737–1742. [https://doi.org/10.1016/S0022-3697\(03\)00122-7](https://doi.org/10.1016/S0022-3697(03)00122-7)
- Lorenz M, Wagner G, Rahm A, Schmidt H, Hochmuth H, Schmid H, Mader W, Brandt M, Von Wenckstern H, Grundmann H (2008) Homoepitaxial ZnO thin films by PLD: structural properties. *Phys Status Solidi (C)* 5(10):3280–3287. <https://doi.org/10.1002/pssc.200779504>
- Säuberlich F, Fritsche J, Hunger R, Klein A (2003) Properties of sputtered ZnO films and its interfaces with CdS. *Thin Solid Films* 431:378–381. [https://doi.org/10.1016/S0040-6090\(03\)00251-7](https://doi.org/10.1016/S0040-6090(03)00251-7)
- Fujihara S, Suzuki A, Kimura T (2003) Ga-doping effects on electrical and luminescent properties of ZnO:(La, Eu)OF red phosphor thin films. *J Appl Phys* 94(4):2411–2416. <https://doi.org/10.1063/1.1594817>
- Chen P, Ma X, Yang D (2007) ZnO:Eu thin-films: Sol–gel derivation and strong photoluminescence from $^5\text{D}_0 \rightarrow ^7\text{F}_0$ transition of Eu^{3+} ions. *J Alloys Compd* 431(1):317–320. <https://doi.org/10.1016/j.jallcom.2006.05.078>
- Kasuga M, Takano T, Akiyama S, Hiroshima K, Yano K, Kishio K (2005) Growth of ZnO films by MOCVD in high magnetic field. *J Cryst Growth* 275(1):1545–1550. <https://doi.org/10.1016/j.jcrysgro.2004.11.189>
- Raji R, Akhilesh Kumar RG, Gopchandran KG (2019) Influence of local structure on luminescence dynamics of red emitting ZnO-Eu³⁺ nanostructures and its Judd-Ofelt analysis. *J Lumin* 205:179–189. <https://doi.org/10.1016/j.jlumin.2018.09.002>
- Zhang Y, Liu Y, Wu L, Xie E, Chen J (2009) Photoluminescence and ZnO \rightarrow Eu^{3+} energy transfer in Eu^{3+} -doped ZnO nanospheres. *J Phys D: Appl Phys* 42:085106–108519. <https://doi.org/10.1088/0022-3727/42/8/085106>
- Cheng B, Yu L, Chang-Kui D, Wang H, Tanner PA (2008) Vacuum ultraviolet and visible spectra of ZnO:Eu³⁺ prepared by combustion synthesis. *J Phys: Condens Matter* 20:34523–34530. <https://doi.org/10.1088/0953-8984/20/34/345231>

33. Zeng X, Yuan J, Wang J, Zhang J (2012) Ferromagnetism in Tb doped ZnO nanocrystalline films. *J Appl Phys* 111:113704–113711. <https://doi.org/10.1063/1.4720381>
34. Yu X, Ma J, Ji F, Wang Y, Zhang X, Cheng C, Ma H (2005) Investigation on doping dependency of solution-processed Ga-doped ZnO thin film transistor. *J Cryst Growth* 274:474–480. <https://doi.org/10.1063/1.2976309>
35. Fujimura N, Nishihara T, Goto S, Xu J, Ito T (1993) The effects of Xe on an rf plasma and growth of ZnO films by rf sputtering. *J Cryst Growth* 130:269–276. <https://doi.org/10.1063/1.1682682>
36. Bachir S, Sandouly C, Kossanyi J, Ronfard-Haret JC (1996) Selective enhancement of blue electroluminescence from GaN:Tm. *J Phys Chem Solids* 5:1869–1875. <https://doi.org/10.1063/1.124958>
37. Jadwisnienczak W, Lozykowski H, Xu A, Patel B (2002) Visible emission from ZnO doped with rare-earth ions. *J Electron Mater* 31:776–784
38. Fujihara S, Sasaki C, Kimura T (2001) Effects of Na content on the luminescence behavior, conduction type, and crystal structure of Na-doped ZnO films. *J Eur Ceram Soc* 21:2109–2118. <https://doi.org/10.1063/1.3603033>
39. Barret C, Massalaski J (1980) Structure of metals. Pergamon press, Oxford, p 1923
40. Deokate R, Pawar S, Moholkar A, Sawant V, Pawar C, Bhosale C, Rajpure K (2008) Effect of trisodium citrate concentration on the structural and photodiode performance of CdO thin film. *Appl Surf Sci* 254:2187–2195. <https://doi.org/10.1016/j.apsusc.2007.09.006>
41. Zhou H, Li Z (2005) Synthesis of nanowires, nanorods and nanoparticles of ZnO through modulating the ratio of water to methanol by using a mild and simple solution method. *Mater Chem Phys* 89:326–331. <https://doi.org/10.1016/j.matchemphys.2004.09.006>
42. Hu J, Gordan RG (1992) Deposition of boron doped zinc oxide films and their electrical and optical properties. *J Electrochem Soc* 139:2014–2022. <https://doi.org/10.1149/1.2221166>
43. Gerigk M, Ehrenreich P, Wagner MR, Wimmer I, Reparaz JS, Sotomayor Torres CM, Schmidt-Mende L, Polarz S (2015) Nanoparticle shape anisotropy and photoluminescence properties: Europium containing ZnO as a model case. *Nanoscale* 7:16969–16982. <https://doi.org/10.1039/C5NR02550H>
44. Han N, Gao X, Lu G, Zeng D, Wan X, Tie S, Lan S (2017) Novel rod- $Y_2O_3:Eu^{3+}@0.01YVO_4:Eu^{3+}$ with open core/shell nanostructure and “off-and-on” fluorescent performance. *RSC Adv* 7:52955–52961. <https://doi.org/10.1039/C7RA08905H>
45. Wang F, Xue X, Liu X (2008) Multicolor tuning of (Ln, P)-doped YVO₄ nanoparticles by single-wavelength excitation. *Angew Chem Int Ed Engl* 47:906–909. <https://doi.org/10.1002/anie.200704520>
46. Engelsen D, Fern GR, Ireland TG, Harris PG, Hobson PR, Lipman A, Dhillon R, Marsha PJ, Silver J (2016) Ultraviolet and blue cathodoluminescence from cubic Y₂O₃ and Y₂O₃:Eu³⁺ generated in a transmission electron microscope. *J Mater Chem C* 4:7026–7034. <https://doi.org/10.1039/C6TC01750A>
47. Wang W, Cheng Z, Yang P, Hou Z, Li C, Li G, Dai Y, Lin J, (2011) Patterning of YVO₄:Eu³⁺ Luminescent films by soft lithography. *Adv Funct Mater* 21:456–463. <https://doi.org/10.1002/adfm.201001467>

Publisher's Note Springer Nature remains neutral with regard to jurisdictional claims in published maps and institutional affiliations.